Am J Transl Res 2024;16(9):4320-4342
www.ajtr.org /ISSN:1943-8141/AJTR0156461

Original Article

Identification of molecular targets and underlying mechanisms of Fuzheng Shengbai Decoction against colon cancer based on network pharmacology

Yu Wang[1*], Shuiming Wang[2*], Min Li[3], Qijia Zhang[4], Mingzhi Fang[3], Qin Zheng[4]

[1]Department of Oncology, Nanjing Hospital of Chinese Medicine Affiliated to Nanjing University of Chinese Medicine, Nanjing 210022, Jiangsu, China; [2]Department of Proctology, Nanjing Hospital of Traditional Chinese Medicine, Nanjing 210022, Jiangsu, China; [3]Department of Oncology, Nanjing Hospital of Traditional Chinese Medicine, Nanjing 210022, Jiangsu, China; [4]Department of Oncology, The Second Hospital of Nanjing, Affiliated to Nanjing University of Chinese Medicine, Nanjing 210003, Jiangsu, China. [*]Equal contributors.

Received March 9, 2024; Accepted July 16, 2024; Epub September 15, 2024; Published September 30, 2024

Abstract: Objectives: To investigate the molecular targets and underlying mechanisms of Fuzheng Shengbai Decoction (FZSBD) against colon cancer (CC). Methods: Multiple network pharmacology approaches were used to predict the molecular targets and underlying mechanisms of FZSBD against CC. The expression of potential molecular targets was determined. The effects of FZSBD on cell viability, proliferation, migration, invasion, and the cell cycle of CC cells were investigated. The therapeutic efficacy, hematological, immunological, and inflammatory data in patients with CC were evaluated after treatment with the XELOX regimen with and without FZSBD. Results: A total of 912 potential targets in FZSBD and 2765 DEGs in CC specimens were screened. Five hub genes (TP53, MYC, VEGFA, CCND1, and IL1B) closely associated with immune-related signaling pathways and the cell cycle process were identified. The five hub genes were of prognostic value in CC. The gene and protein expression of the five hub genes was significantly higher in CC tumor tissue samples than that of normal tissue samples. Furthermore, with increasing doses, FZSBD increasingly inhibited growth, migration, and invasion, and suppressed the cell cycle process of CC cells. Supplementing of FZSBD to the XELOX regimen enhanced immune modulation and alleviated inflammatory responses. Conclusions: This study identified the molecular targets and underlying mechanisms of FZSBD treatment against CC and may provide clues for future research on the treatment of CC with FZSBD.

Keywords: Fuzheng Shengbai Decoction, colon cancer, network pharmacology, inflammatory response

Introduction

Colon cancer (CC), the fifth most commonly diagnosed malignancy, is characterized by uncontrolled cell growth in the colon or rectum. In 2020, a total of 576,858 CC deaths were reported, accounting for 5.8% of all cancer-related deaths, and represents a great threat to human health [1]. Despite the availability of valid treatment approaches to achieve curative effects (i.e. surgery, chemotherapy, radiotherapy, and targeted therapies on CC in the clinic), the prognosis of CC is poor and the overall five-year survival of patients with CC is below 38% [2, 3]. Therefore, it is essential to explore effective therapies and the related molecular targets and underlying mechanisms to improve the clinical treatment of CC.

Traditional Chinese medicine (TCM) has attracted increasing attention for its efficacy and minimal side effects in cancer treatment [4-6]. Fuzheng Shengbai Decoction (FZSBD) was developed at our hospital as a clinical prescription, consisting of *Astragalus membranaceus* (Huangqi), *Psoralen corylifolia L.* (Buguzhi), *Cervi Cornus Colla* (Lujiaojiao), *Codonopsis pilosula* (Dangshen), *Fructus Ligustri Lucidi* (Nvzhenzi), *Asini Corii Colla* (Ejiao), *Angelicae Sinensis Radix* (Danggui), *Caulis Spatholobi* (Jixueteng), and *Fructus amomi* (Sharen). FZSBD is commonly applied in the clinical treatment of CC.

https://doi.org/10.62347/VKMZ3204

Multiple active ingredients in *Astragalus membranaceus*, such as polysaccharides, saponins, and flavonoids, effectively suppress the progression of CC mainly by inhibiting the proliferation, invasion, and migration of CC, promoting apoptosis and the inflammatory response of CC, enhancing the body's immune function, and preventing endoplasmic reticulum stress-induced intestinal cell damage [7-9]. Recently, *Psoralen corylifolia L.* has been shown to possess good therapeutic prospects for multiple cancers, such as breast, liver, prostate, and colon cancer, by inducing apoptosis and cell cycle arrest, increasing reactive oxygen species to induce autophagy, inhibiting migration, invasion, and bone metastasis [10]. The active compounds in *Codonopsis pilosula*, polysaccharides, also exhibit excellent inhibitory effects in various cancers, including ovarian cancer and hepatocellular carcinoma [11, 12]. Beta-sitosterol, a dominant ingredient of *Fructus Ligustri Lucidi*, can induce cell-cycle arrest and enhance the immune system to inhibit cancer progression [13, 14]. Hydrolysate compounds from *Asini Corii Colla* possess antioxidant ability and promote hematopoietic and immune functions to suppress cancers [15, 16]. Most ingredients in *Angelicae Sinensis Radix*, such as ferulic acid, polysaccharides, and volatile oils, possess inhibitory effects on various tumors [17, 18]. The extracts from the *Caulis Spatholobi*, especially the total flavonoid extract, also exhibit anti-tumor activity *in vivo* and *in vitro* [19, 20]. Although the anti-tumor effects of most Chinese materia medica that constitute FZSBD are clear, the underlying mechanisms of our preparation of FZSBD remain elusive.

Network pharmacology, a systematic approach for predictive analysis, predicts a correlation between effective ingredients and their corresponding target genes by establishing a multilevel network, such as a drugs-components-targets-disease network [21]. Complex ingredients with multiple pathologic target genes and underlying pathways have been implicated in TCM recipes, and the application of network pharmacology is well-suited for the analysis of multi-ingredient, multi-channel, and multi-target synergy in TCM [22-24]. Based on bioinformatics, network pharmacology shows potential in the investigation of promising therapeutic targets and underlying mechanisms of specific drugs in cancer treatment [25-27].

In this study, we aimed to identify the molecular targets and underlying mechanisms of FZSBD in the treatment of CC by combining bioinformatics and network pharmacology with *in vitro* studies and clinical practice. Our findings may provide evidence for the application of FZSBD in the treatment of patients with CC.

Materials and methods

Admission criteria and ethics statement

All experimental clinical protocols in this study involving patients with CC were approved by the Institutional Review Board of Nanjing Hospital of Traditional Chinese Medicine (accession number: KY2023311). Eligibility criteria were stringently determined before patient enrollment in the study and included: 1) patients who were diagnosed with CC through pathologic diagnosis; 2) patients who were ineligible for surgery; 3) patients with Karnofsky performance scale (KPS) >90, who could tolerate chemotherapy; 4) patients with no contraindications to chemotherapy; and 5) patients with an expected survival more than 3 months. The exclusion criteria were: 1) patients who did not meet the diagnostic criteria; 2) patients with vital organ dysfunction who could not tolerate chemotherapy; and 3) female patients who were pregnant or breastfeeding. The written informed consent was obtained from all participants before any procedure or sample collection, and these data were anonymized and stored in a secure electronic database to ensure patient confidentiality.

Patients and clinical specimens

A total of 46 patients diagnosed with advanced CC in our hospital from January 2019 to March 2023 were selected and divided into the XELOX group and the XELOX + FZSBD group (n = 23 each). The patient characteristics are presented in **Table 1**, which show negligible differences (P>0.05). The patients underwent chemotherapy following the XELOX regimen, including capecitabine (Roche Pharmaceuticals, Shanghai, China) at a dose of 1250 mg/m^2, twice daily for 14 days, supplemented with oxaliplatin (Hengrui Medicine, Jiangsu, China) at a dose of 130 mg/m^2 on the first day and the 21st day, repeated every 21 days for a total of four cycles. In addition to the XELOX regimen, the XELOX + FZSBD group received FZSBD at a

Table 1. Baseline demographics and clinical characteristics of patients with colon cancer (CC)

Characteristic	XELOX	XELOX + FZSBD	χ^2	*P*-value
Age (years)	58.6 ± 10.2	59.1 ± 9.8		0.846
Gender			0.045	0.782
Male, n (%)	13 (56.5)	14 (60.9)		
Female, n (%)	10 (43.5)	9 (39.1)		
BMI	25.3 ± 3.8	25.5 ± 4.1		0.904
Histological type			0.241	0.623
AC, n (%)	20 (87.0)	19 (82.6)		
MAC, n (%)	3 (13.0)	4 (17.4)		
Tumor location			2.428	0.297
Right colon (%)	10 (43.5)	11 (47.8)		
Left colon (%)	8 (34.8)	5 (21.7)		
Rectum (%)	5 (21.7)	7 (30.4)		
Tumor stage				
III (%)	23 (100)	23 (100)		
Tumor grade			3.352	0.187
Low (%)	3 (13.0)	4 (17.4)		
Moderate (%)	13 (56.5)	15 (65.2)		
High (%)	7 (30.4)	4 (17.4)		
Performance status			0.422	0.561
0-1 (%)	14 (60.9)	12 (52.1)		
2-3 (%)	9 (39.1)	11 (47.8)		
Comorbidities, n (%)			0.196	0.658
Hypertension	7 (30.4)	6 (26.1)		
Diabetes	3 (13.0)	4 (17.4)		

Notes: n = 23 each group. Quantitative data were expressed as mean ± SD. AC, adenocarcinoma; MAC, mucinous adenocarcinoma.

dose of 20 mL, taken three times daily for 3 months. Blood samples were obtained before and after treatment from subjects by using a 21-gauge needle and BD Vacutainer® tubes (BD Biosciences, Franklin Lakes, NJ, USA). Subsequently, the collected blood was centrifuged at 3000 rpm for 10 min to separate the sera.

Therapeutic efficacy assessment

The efficacy of the two regimens was evaluated by complete response (CR), partial response (PR), stable disease (SD), disease control rate (DCR), objective response rate (ORR), and bone marrow suppression (BMS) of the patients from January 2019 to March 2023. CR represents the complete disappearance of CC after treatment. PR is defined as at least a 30% decrease in the sum of diameters of target lesions compared to baseline. SD indicates that CC has neither significantly decreased nor significantly increased. DCR is the total proportion of CR, PR, and SD. ORR is defined as the total ratio of CR and PR, and BMS refers to a decrease in the ability of the bone marrow to produce blood cells.

Complete blood count test

Complete blood count data in patients with CC, including white blood cells (WBCs), red blood cells (RBCs), platelets (PLTs), and hemoglobin (HB), were determined by using a Sysmex XN-1000 hematology analyzer (Sysmex Corporation, Kobe, Japan) from April 2023 to June 2023. The analyzer was calibrated daily and control samples were run for quality assurance before testing the patient samples. The manufacturer's recommended protocols and reagents were strictly followed.

Flow cytometry

The immune microenvironment of the patients was determined from July 2023 to September 2023 with the help of flow cytometry. Peripheral blood mononuclear cells (PBMCs) were isolated from blood samples of patients by using density-gradient centrifugation with Ficoll-Paque PLUS (GE Healthcare, Uppsala, Sweden). The PBMCs were then washed twice with phosphate buffer solution (PBS) and resuspended in flow cytometry staining buffer. For surface staining, cells were incubated with the following fluorochrome-conjugated monoclonal antibodies: anti-CD3-FITC, anti-CD4-PE, and anti-CD8-APC (all antibodies were purchased from BD Biosciences, San Jose, CA, USA) for 30 min at 4°C in the dark. After washing with PBS, cells were fixed with 1% paraformaldehyde (Sigma-Aldrich, St. Louis, MO, USA). The cell cycle of CC cells was determined from December 2022 to January 2023 with the help of flow cytometry. The treated CC cells were harvested and fixed with 75% ethanol overnight, followed by incubation with propidium iodide (50 μg/ml, Thermo Fisher) for 30 min at 37°C in the dark. Next, the proportion of T cell subsets or the relative ratios of the

G0/G1, S, and G2/M phases of CC cells were examined by flow cytometry (Thermo Fisher) and FlowJo software (BD Biosciences, USA) was used for the analyses.

Enzyme-linked immunosorbent assays (ELISA)

Serum levels of carcinoembryonic antigen (CEA, a marker used to monitor the therapeutic efficacy of CC), C-reactive protein (CRP), interleukin-6 (IL-6), tumor necrosis factor-α (TNF-α), and IL-1β in patients with CC were determined by using ELISA kits from November 2023 to December 2023. ELISA kits for CEA (HM10223), CRP (KHA0031), IL-6 (BMS213HS), TNF-α (88-7346-88), and IL-1β (BMS224-2) were obtained from Invitrogen (Waltham, MA, USA). The assays were performed strictly according to the manufacturer's instructions. The optical density was measured at 450 nm and the concentration of the cytokines and CRP in the serum were calculated from standard curves.

Identification of active components and target genes for FZSBD

From December 2020 to January 2021, active components of FZSBD were respectively searched in the Traditional Chinese Medicine systems pharmacology (TCMSP) platform (http://lsp.nwu.edu.cn/tcmsp.php) [28], the HERB platform (http://herb.ac.cn/) [29], and the bioinformatics analysis tool for molecular mechANism (BATMAN) platform (http://bionet.ncpsb.org/batman-tcm/) [30]. Candidate target genes for the active components of FZSBD were also predicted from the TCMSP, HERB, and BATMAN platforms. UniProt (http://www.UniProt.org/) database was applied for the conversion of target gene names to official symbol formats.

Construction of a component-target network of FZSBD

In February 2021, Cytoscape software version 3.8.1 (https://cytoscape.org) was applied to construct drug-target networks for active components in the FZSBD to explore its pharmacological mechanisms.

Analysis of differentially expressed genes

From April 2021 to May 2021, RNA-seq data of gene expression in CC tissues and normal tissues were obtained from the Gene Expression Omnibus (GEO) database (www.ncbi.nlm.nih.gov/geo/) (GSE10972) on the GPL6104 platform. Differentially expressed genes (DEGs) were selected using the Limma package under the screening condition of |logFC|>1 and adjusted *P* value <0.05. The visualization of volcano plots and heat maps was achieved with the ggplot2 and pheatmap packages in R software.

Gene set enrichment analysis (GSEA)

In July 2021, the underlying biological functions associated with the significant DEGs in CC were explored by using the R package and the clusterProfiler package in the GESA. Adjusted *P*-value of <0.05 and false discovery rate Q-value of <0.25 indicated significance.

Gene Ontology and Kyoto Encyclopedia of Genes and Genomes

In September 2021, the packages 'clusterProfiler', 'enrichplot', and 'ggplot2' in the R software were applied for the Gene Ontology (GO) and Kyoto Encyclopedia of Genes and Genomes (KEGG) enrichment analyses. Three modules were selected for the GO enrichment analyses, including biological process, cell composition, and molecular function.

Correlation analysis of hub gene levels and immune cell infiltration

From October 2021 to November 2021, an immune infiltration analysis was conducted with GSEA by applying the GSVA package in R software. The proportion of 24 tumor-infiltrated immune cell types was determined and Spearman's correlation analysis was performed to analyze the correlation between the expression of hub genes and the degree of immune cell infiltration. The pheatmap packages in R software were used to visualize the heat maps. The package 'estimate' in R software was applied to evaluate the immune-stromal components in the tumor microenvironment, and three scores, including the immune score (infiltration level of immune cells), stromal score (stromal amount), and the ESTIMATE score (both) were calculated. The higher the score, the larger the ratio of the corresponding component in the tumor microenvironment.

Construction of protein-protein interaction networks

In December 2021, protein-protein interaction (PPI) networks of drug-disease targets were

built based on the STRING database (https://string-db.org/). The degree of gene interactions in the PPI network was calculated by the cytoHubba plugin for hub gene extraction from PPI networks. The molecular complex detection (MCODE) on the Cytoscape software was applied for the selection of representative modules.

Preparation of FZSBD

FZSBD is composed of nine natural medicinal components, including *Astragalus membranaceus* (Huangqi, 45 g), *Psoralen corylifolia L.* (Buguzhi, 90 g), *Cervi Cornus Colla* (Lujiaojiao, 30 g), *Codonopsis pilosula* (Dangshen, 30 g), *Fructus Ligustri Lucidi* (Nvzhenzi, 30 g), *Asini Corii Colla* (Ejiao, 30 g), *Angelicae Sinensis Radix* (Danggui, 30 g), *Caulis Spatholobi* (Jixueteng, 90 g), and *Fructus amomi* (Sharen, 6 g). In January 2022, the decoction was prepared from high-quality products selected by experienced herbalists and transformed into lyophilized powder in light of a general preparation procedure [31]. A 500 mg sample of FZSBD lyophilized powder was precisely weighed and dissolved in 10 mL of PBS to prepare the FZSBD solution at a final concentration of 50 mg/mL. The original concentration was diluted to the required concentrations (0.25, 0.5, 0.75, 1, 1.5, 2 mg/mL) for subsequent experiments.

Cell culture and treatment

In March 2022, human CC cell lines (HCT8, #CCL-244; SW48, #CCL-231; LoVo, #CCL-229; HCT116, #CCL-247) were purchased from the American Type Culture Collection (ATCC, USA) and incubated in Dulbecco's modified Eagle medium (DMEM, Sigma-Aldrich). Colon epithelial cells (NCM460, #AW-CCH306) were purchased from Abiowell (Changsha, China) and incubated in RPMI-1640 medium (Thermo Fisher). The cell culture medium contained 10% fetal bovine serum (FBS) and 1/100 penicillin-streptomycin and cells were cultured under 5% CO_2 at 37°C.

Methylthiazolyldiphenyl-tetrazolium bromide assay

The methylthiazolyldiphenyl-tetrazolium bromide (MTT) assay was performed from April 2022 to June 2022. All CC cells were grown in a 96-well plate and received treatment with 0.25, 0.5, 0.75, 1, 1.5, and 2 mg/mL FZSBD at 37°C for 36 h. An MTT cell growth assay kit (Sigma-Aldrich) was applied to examine the impact of FZSBD on CC cells following the manufacturer's protocol. Each well was added with 10 μL of MTT reagent and cultured for another 4 h. Next, 100 μL of dimethyl sulfoxide was supplemented into each well to solubilize Formazan. Infinite M200 (Tecan) was applied to evaluate the absorbance of CC cells at 570 nm and the half-maximal inhibitory concentration (IC_{50}) value was calculated.

Wound healing assay

The wound healing assay was performed in July 2022. All CC cells were treated with a low dose (0.75 mg/mL) and a high dose (1.5 mg/mL) of FZSBD. Cells were grown in a 6-well plate (1×10^5 cells per well) and cultured to 80% confluence. A pipette tip was then used to scratch the cell monolayer, followed by washing with PBS three times. An Olympus microscope was used to capture the images of CC cells at 0 h and 24 h. The rate of wound healing was defined as the ratio between the migration distance and the original distance.

Transwell assay

The Transwell assay was performed in August 2022. Transwell chambers coated with matrix gel were placed in a culture plate. All treated CC cells suspended in DMEM without FBS at a concentration of 1×10^5 cells/mL were inoculated into the apical chamber, and complete culture media was supplemented into the chamber at the bottom. The uninvaded cells on the membrane surface of the apical chambers were cleaned with a cotton swab after 24 h. Subsequently, the invaded cells were dyed by using 0.1% crystal violet (Beyotime), and their number was counted under a microscope (Olympus).

Colony formation assay

The colony formation assay was performed in September 2022. The treated CC cells were inoculated into 12-well plates and incubated in a complete medium at 37°C for two weeks. The cells were fixed by using 4% paraformaldehyde for 60 min and then stained with 2% crystal violet (Beyotime). The images in each group were captured with a light microscope and the colo-

ny number was manually counted in three randomly selected visual fields.

Real-time quantitative PCR

Real-time quantitative PCR (RT-qPCR) was performed from October 2022 to December 2022. The TRIzol kit (Omega, USA) was used to isolate total RNA in treated CC cells. cDNA synthesis was performed with MultiScribe Reverse Transcriptase (Applied Biosystems). PCR was carried out by using the SYBR Green PCR Master Mix (Takara, Japan) on the StepOne Plus Real-Time PCR System. Relative mRNA expression level was determined by using the $2^{-\Delta\Delta Ct}$ method, and GAPDH was the internal control. The used primer sequences were as follows.

TP53: Forward: 5'-CTCAGATAGCGATGGTCTGG-3', Reverse: 5'-CTGTCATCCAAATACTCCACAC-3'; MYC: Forward: 5'-ATTCTCTGCTCTCCTCGAC-3', Reverse: 5'-TTGTTCCTCCTCAGAGTCG-3'; VEGFA: Forward: 5'-ATCTTCAAGCCATCCTGTG-3', Reverse: 5'-TTTACACGTCTGCATGGTG-3'; CCND1: Forward: 5'-CATTGAACACTTCCTCTCCA-3', Reverse: 5'-AACTTCACATCTGTGGCAC-3'; IL1B: Forward: 5'-GCTTATTACAGTGGCAATGAGG-3', Reverse: 5'-AGATTCGTAGCTGGATGCC-3'; GAPDH: Forward: 5'-CCTCCTGTTCGACAGTCAG-3', Reverse: 5'-CATACGACTGCAAAGACCC-3'.

Western blotting

Western blotting was performed from October 2022 to December 2022. Total proteins from treated CC cells were extracted by using RIPA solution (GenePharma). A BCA protein assay kit (Beyotime) was used to determine protein concentration. Protein samples were separated by SDS-PAGE and then electro-transferred onto polyvinylidene fluoride membranes, which were subsequently blocked with 5% fat-free milk and cultured with anti-TP53 (ab32389, 1:10,000, Abcam), anti-MYC (ab32072, 1:1,000, Abcam), anti-VEGFA (ab214424, 1:1,000, Abcam), anti-CCND1 (ab16663, 1:200, Abcam), anti-IL1B (ab2105, 1:2,000, Abcam), and anti-GAPDH (ab245355, 1:5,000, Abcam) overnight at 4°C, among which GAPDH was the loading control. The membranes were then co-cultured with the corresponding secondary antibodies for 60 min at ambient temperature. The blots were visualized by using an enhanced chemiluminescence system (Roche), and the quantification of the target bands was performed with ImageJ software.

Statistical analysis

The statistical analysis was performed in January 2024. All data produced in clinical samples were used for statistical analysis afyter the inclusion and exclusion criteria were performed. Incidental data generated from cellular experiments were excluded before being used for statistical analysis. GraphPad Prism v.8.0 was applied for analysis and the results were displayed as mean ± SD. The difference between groups was analyzed by using Student's t-test. The ANOVA test was applied for the comparison of more than two groups. Tukey's test was performed for mutual *post hoc* pairwise comparison of groups. $P<0.05$ indicated statistical significance.

Results

Active components and potential targets of FZSBD

A total of 109 active components of the nine constituents in FZSBD were predicted based on TCMSP, HERB, and BATMAN databases, and the drug-component-target network was established. There were 20 active components of Huangqi with 472 targets (**Figure 1A**), 14 active ingredients of Buguzhi with 274 targets (**Figure 1B**), 2 active components of Lujiaojiao with 13 targets (**Figure 1C**), 21 active components of Dangshen with 284 targets (**Figure 1D**), 13 active ingredients of Nvzhenzi with 401 targets (**Figure 1E**), 3 active components of Ejiao with 400 predicted targets (**Figure 1F**), 2 active ingredients of Dangui with 100 targets (**Figure 1G**), 24 active components of Jixueteng with 576 predicted targets (**Figure 1H**), and 10 active components of Sharen with 240 targets (**Figure 1I**). After deleting repetitive targets, 912 targets were selected for the FZSBD.

DEGs in CC and shared targets with FZSBD

The DEGs in CC were explored based on the analysis of the GEO database (GSE10972). As shown in the principal component analysis and the uniform manifold approximation and projection plots, a significant difference could be found between group 1 (normal tissue samples) and group 2 (CC tumor samples) (**Figure 2A**,

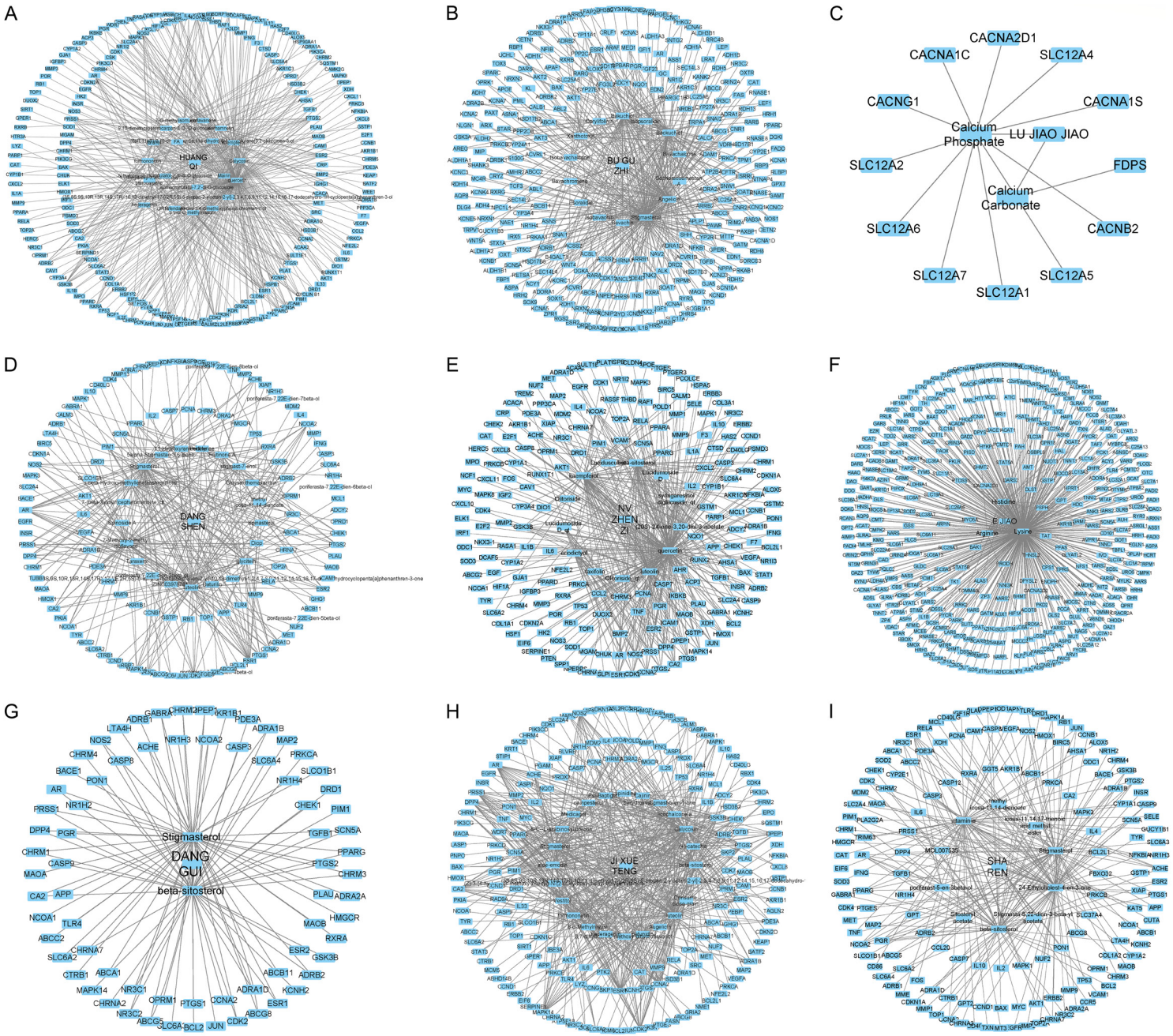
A
HUANG QI
B
BU GU ZHI
C
CACNA2D1
CACNA1C
SLC12A4
CACNG1
CACNA1S
Calcium Phosphate
LU JIAO JIAO
SLC12A2
FDPS
Calcium Carbonate
SLC12A6
CACNB2
SLC12A7
SLC12A5
SLC12A1
D
DANG SHEN
E
NV ZHEN ZI
F
E JIAO
Arginine
Lysine
G
Stigmasterol
DANG GUI
beta-sitosterol
H
JI XUE TENG
I
SHA REN

Figure 1. Active components and potential targets of Fuzheng Shengbai Decoction (FZSBD). The drug-component-target network for (A) Huangqi, (B) Buguzhi, (C) Lujiaojiao, (D) Dangshen, (E) Nvzhenzi, (F) Ejiao, (G) Dangui, (H) Jixueteng, and (I) Sharen were constructed by using Cytoscape software. The edges indicate the interaction between active components and predicted targets, and the node size represents the degree of interaction.

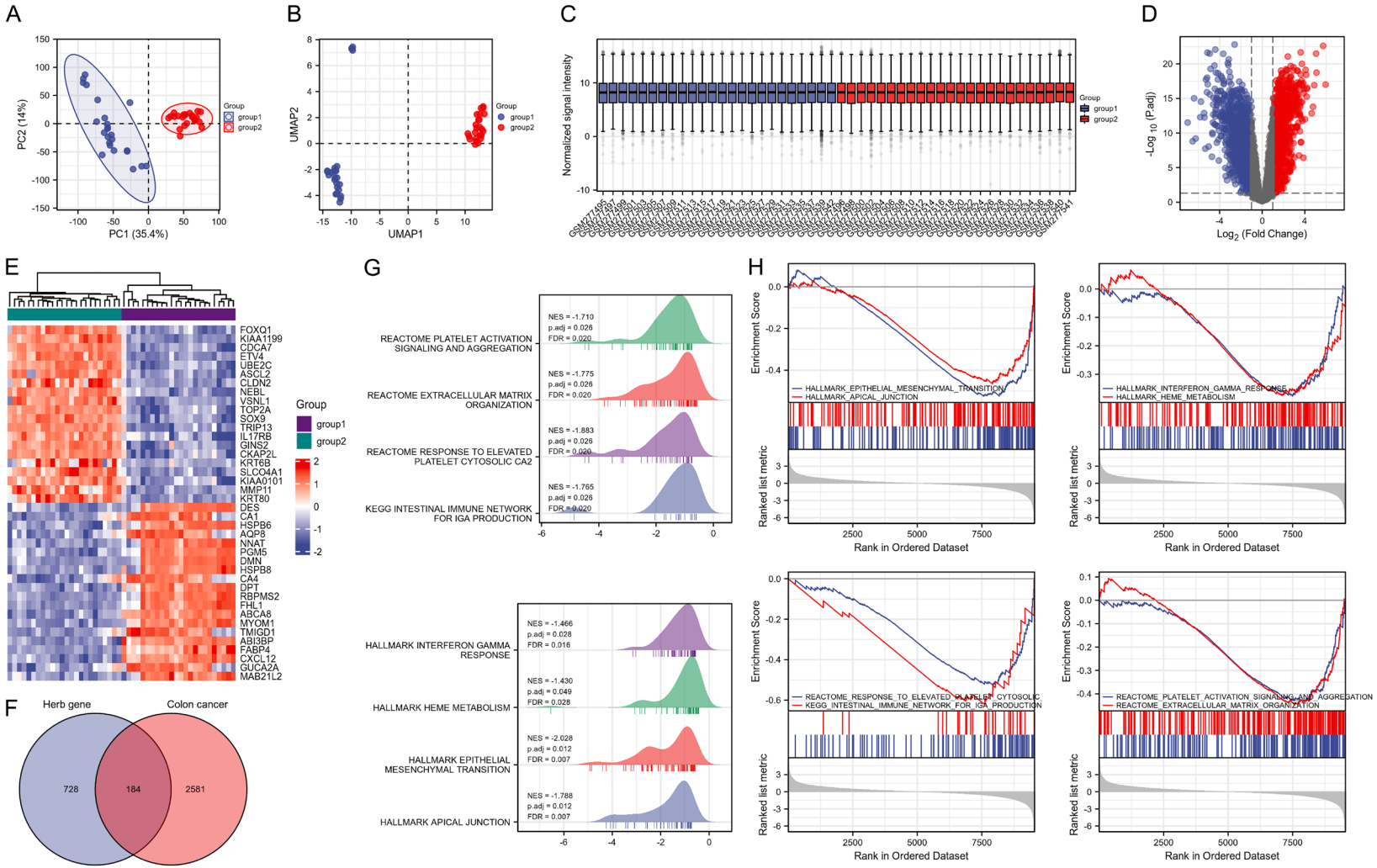

Figure 2. Identification of differentially expressed genes (DEGs) in colon cancer (CC) and drug-disease targets. (A) Principal component analysis and (B) uniform manifold approximation and projection plots of group 1 (normal tissue samples) and group 2 (CC tumor samples) based on the Gene Expression Omnibus (GEO)

database (GSE10972). (C) Box plot of normalized data in groups 1 and 2. (D) Volcano plot of DEGs in CC in the GEO database (GSE10972) under the condition of logFC>1 and adjusted *P* value <0.05. Red indicates the up-regulated genes and blue represents the down-regulated genes. (E) Heat map of the top 20 up-regulated genes and top 20 down-regulated genes in CC. (F) Venn diagram of the intersected genes between targets of active components in FZSBD and the DEGs in CC. (G, H) Gene set enrichment analysis (GSEA) showed the enrichment of drug-disease targets in hallmark pathways.

2B). The data were then normalized, standardized, and presented in **Figure 2C**. A total of 2,765 DEGs were filtered under the condition of |logFC|>1 and adjusted *P* value <0.05, among which 1,364 were up-regulated genes and 1,401 were down-regulated genes (**Figure 2D**). The 20 highest-regulated genes and the 20 lowest-regulated genes in CC are shown in **Figure 2E**. Then the predicted targets of the active components in FZSBD were intersected with the DEGs in CC and 184 target genes were selected from the overlapped area (**Figure 2F**). GSEA was performed based on the 184 drug-disease targets, and the results revealed that the drug-disease targets were significantly enriched in platelet activation signaling and aggregation, extracellular matrix organization, response to elevated platelet cytosolic CA2, intestinal immune network for IGA production, interferon gamma response, HEME metabolism, epithelial-mesenchymal transition, and apical junction (**Figure 2G**, **2H**).

PPI networks and functional enrichment analyses

The PPI network of drug-disease targets was built by using the STRING database (**Figure 3A**). The cytohubba plug-in was used to calculate the degree of drug-disease targets in the PPI network and color them according to the corresponding degrees. After being classified by using the Degree method, TP53, MYC, VEGFA, CCND1, and IL1B were selected as the top five targets (**Figure 3B**). The MCODE plug-in was used for cluster analysis and extraction of three representative modules from the PPI network, presented as **Figure 3C-E**. Furthermore, KEGG and GO analyses were conducted for the hub genes in the sub-networks. A total of 1,125 items in the three categories of GO analysis were identified, in which 1,005 items belong to biological processes, 36 items belong to cellular components, and 84 items belong to molecular functions. A total of 68 items were identified in the KEGG analysis. The top three enriched items of the three categories of the GO and KEGG analysis were shown as bar charts and bubble charts in **Figure 3F**. The top three enrichment signaling pathways of the hub genes in terms of biological processes, cell composition, and molecular function are listed below. The biological processes included cell cycle arrest, G1/S transition of mitotic cell cycle, and cell cycle G1/S phase transition. The cell composition processes included complex, transferring, phosphorous-containing groups, serine/threonine protein kinase complex, and cyclin-dependent protein kinase, and holoenzyme complex. Molecular function was enriched in kinase regulator activity, protein kinase regulatory activity, and cyclin-dependent protein serine/threonine kinase regulator activity. KEGG analyses indicated these hub genes were abundantly enriched in chronic myeloid leukemia, bladder cancer, and cell cycle (**Figure 3F**).

Expression of the hub genes in CC and the correlation with the immune characteristics

As drug-disease targets were enriched in immune-related signaling based on GSEA analysis, we further evaluated the correlation of TP53, MYC, VEGFA, CCND1, and IL1B levels with immune characteristics. The up-regulated expression of TP53, MYC, VEGFA, CCND1, and IL1B was identified in CC tumor tissue samples compared with normal tissue samples (**Figure 4A**, **4B**). Moreover, the heat map reflected the correlation between TP53, MYC, VEGFA, CCND1, and IL1B with an immune infiltration score of the 24 immune cells. IL1B was mainly positively correlated with immune cells and showed no significant correlation with NK and Tcm cells. TP53 was positively correlated with aDC, cytotoxic cells, NK cells, TFH, Th17 cells, Th2 cells, and TReg cells, and negatively correlated with Tcm. CCND1 was positively correlated with aDC, cytotoxic cells, CD8 T cells, neutrophils, macrophages, NK cells, T helper cells, Tcm, Tem, TFH, Tgd, and Th1 cells, and showed a negative correlation with Th17 cells. MYC was positively correlated with eosinophils, NK cells,

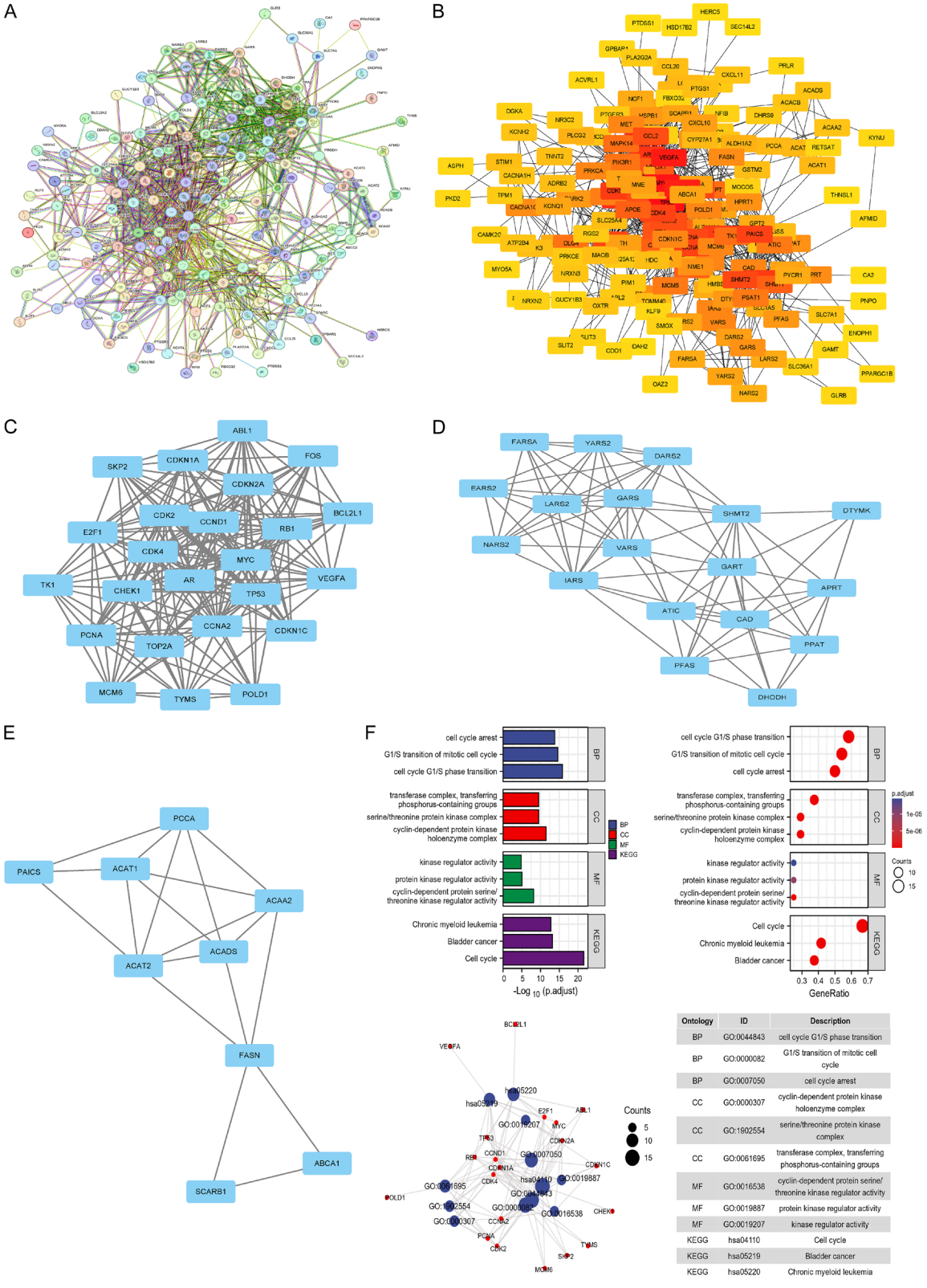

Ontology	ID	Description
BP	GO:0044843	cell cycle G1/S phase transition
BP	GO:0000082	G1/S transition of mitotic cell cycle
BP	GO:0007050	cell cycle arrest
CC	GO:0000307	cyclin-dependent protein kinase holoenzyme complex
CC	GO:1902554	serine/threonine protein kinase complex
CC	GO:0061695	transferase complex, transferring phosphorus-containing groups
MF	GO:0016538	cyclin-dependent protein serine/threonine kinase regulator activity
MF	GO:0019887	protein kinase regulator activity
MF	GO:0019207	kinase regulator activity
KEGG	hsa04110	Cell cycle
KEGG	hsa05219	Bladder cancer
KEGG	hsa05220	Chronic myeloid leukemia

Figure 3. Protein-protein interaction (PPI) network of drug-disease targets and functional enrichment analysis. A. STRING database was used to generate the PPI network of the drug-disease targets. B. The CytoHubba plug-in was used for the selection of hub genes in the PPI network. C-E. Molecular complex detection plug-in was used to select the most significant subnetwork based on cluster analysis. F. Gene Ontology and Kyoto Encyclopedia of Genes and Genomes analysis for the drug-disease targets.

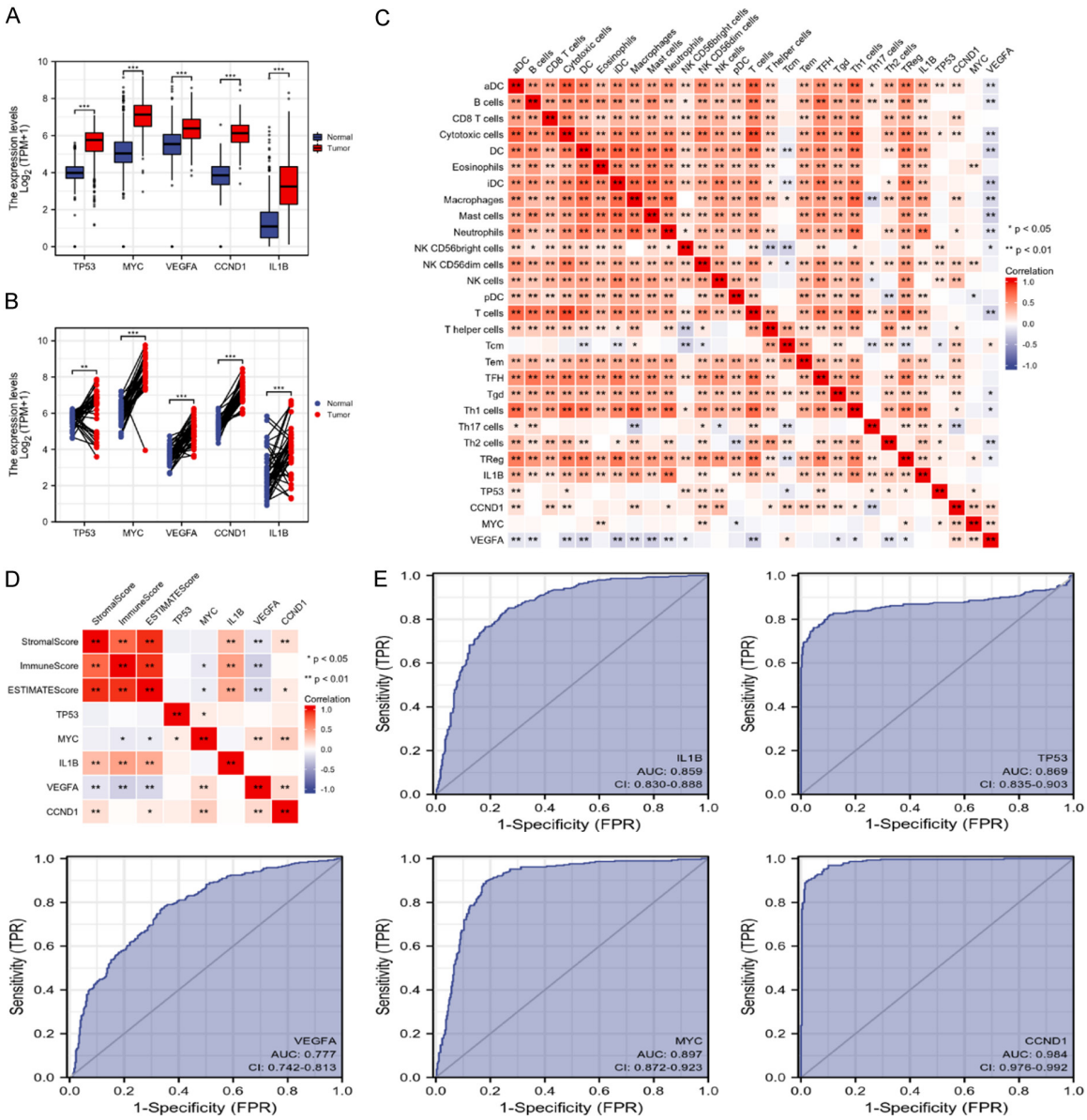

Figure 4. Expression of the hub genes in CC and the correlation with the immune characteristics. The expression of five hub genes in (A) unpaired or (B) paired CC tissue samples, and normal samples. (C) Heat map showing the correlation between the expression the five hub genes and 24 immune cell types. (D) Heat map showing correlation of the expression the five hub genes and stromal, immune, and estimate scores based on the ESTIMATE method. (E) Receiver operating characteristic curves of the sensitivity and specificity for the five hub genes in CC.

and Treg, and showed a negative correlation with pDC cells. VEGFA was mainly negatively associated with immune cells, including aDC, cytotoxic cells, B cells, DC, iDC, mast cells, macrophages, neutrophils, NK cells, T cells, Tgd, Th1 cells, Th2 cells, and Treg, and showed a positive correlation with Tcm (**Figure 4C**). The correlation between the stromal, immune and estimate scores with the expression of five hub genes was then evaluated by using the ESTIMATE method. The heat map suggested that there was no significant correlation between TP53 and the stromal, immune, and estimate scores. MYC was negatively correlated with the immune score or estimate score. IL1B was positively correlated with the stromal, immune, and estimate scores. VEGFA was negatively correlated with the stromal, immune, and estimate scores. CCND1 was positively correlated with the stromal score and estimate

score (**Figure 4D**). The receiver operating characteristic curves indicated that the five hub genes were of prognostic value and may serve as significant biomarkers with diagnostic value for CC. The area under the curve of IL1B was 0.859 (CI: 0.830-0.888), 0.869 for TP53 (CI: 0.835-0.903), 0.777 for VEGFA (CI: 0.742-0.813), 0.897 for MYC (CI: 0.872-0.923), and 0.984 for CCND1 (CI: 0.978-0.992) (**Figure 4E**).

FZSBD inhibited the expression of the hub gene and the viability of CC cells

As shown by the RT-qPCR and western blotting analyses results presented in **Figure 5A**, five hub genes, namely TP53, MYC, VEGFA, CCND1, and IL1B, were highly expressed in colon cancer cell lines (HCT8, SW48, LoVo, HCT116) compared to colon epithelial cells (NCM460). The results of MTT assays revealed that CC cell viability gradually decreased after treatment with FZSBD in a dose-dependent and time-dependent fashion. The IC_{50} values of HCT116 at 24 and 48 h were 0.91 and 0.83 mg/mL, respectively (**Figure 5B**). Next, we evaluated the effects of FZSBD on the expression of five hub genes. The expression levels of TP53, MYC, VEGFA, CCND1, and IL1B were down-regulated by FZSBD in a dose-dependent manner (**Figure 5C-G**).

FZSBD suppressed the proliferation of CC cells

As presented in **Figure 6A**, **6B**, the colony numbers of CC cells were significantly decreased in a dose-dependent way after the administration of FZSBD, indicating that FZSBD exerted suppressive effects on the proliferation of HCT116 and HCT8 cells.

FZSBD hindered CC cell migration and invasion

We explored the impact of FZSBD on the migration and invasion of HCT116 and HCT8 cells. The wound healing distance of CC cells exhibited a significant, dose-dependent reduction in the FZSBD-treated groups, suggesting that FZSBD significantly inhibited the migration of CC cells (**Figure 7A**, **7B**). Furthermore, the number of invaded CC cells also declined significantly in the FZSBD-treated groups, and the number of invaded cells in the high-dose group was the lowest, which indicated that treatment with FZSBD significantly reduced the invasion of CC cells in a concentration-dependent fashion (**Figure 8A**, **8B**).

FZSBD inhibited the cell cycle process of CC cells

The results of the GO and KEGG analysis indicated that the hub genes were closely associated with cell cycle signaling. Next, we examined the impact of FZSBD on the cell cycle of CC cells. According to flow cytometry results, treatment with FZSBD gradually promoted cell cycle arrest in the G0/G1 phase as the concentration increased, suggesting that FZSBD suppressed the cell cycle process of CC cells (**Figure 9A**, **9B**).

FZSBD supplementation modulated the immune microenvironment and inflammatory levels in the serum of patients with CC

As shown in **Table 2**, compared to the XELOX group, the XELOX + FZSBD group showed a decreased CR. Furthermore, BMS in the XELOX + FZSBD group was significantly lower than that of the XELOX group, which indicated that the additional treatment of FZSBD contributed to the reduction of the adverse effects of XELOX. After evaluating the hematological responses of patients with CC undergoing distinct treatment modalities, significant differences were observed between pre-treatment and post-treatment. As **Table 3** shows, following treatment of XELOX and XELOX + FZSB, there was a marked decline in whole blood values, including WBC, RBC, and PLT counts. However, no statistically significant disparities were discerned between the two therapeutic modalities concerning these parameters. Subsequently, T-cell subsets were analyzed by using flow cytometry. As **Table 4** illustrates, in both treatment groups, the expression of $CD3^+$ and $CD4^+$ T cells in the post-treatment group was dramatically elevated compared to the pre-treatment group, but the expression of $CD8^+$ T cells in the post-treatment group declined prominently compared with the pre-treatment group. Intriguingly, the combination of FZSB with the XELOX regimen produced a more substantial increase in $CD3^+$ T cells and a more prominent reduction in $CD8^+$ T cells, suggesting a potential synergistic immunomodulatory role of FZSB. As **Table 5** shows, both treatment regimens effectively reduced the levels of inflammatory markers, including CRP and IL-1β. Meanwhile, combination therapy of XELOX with

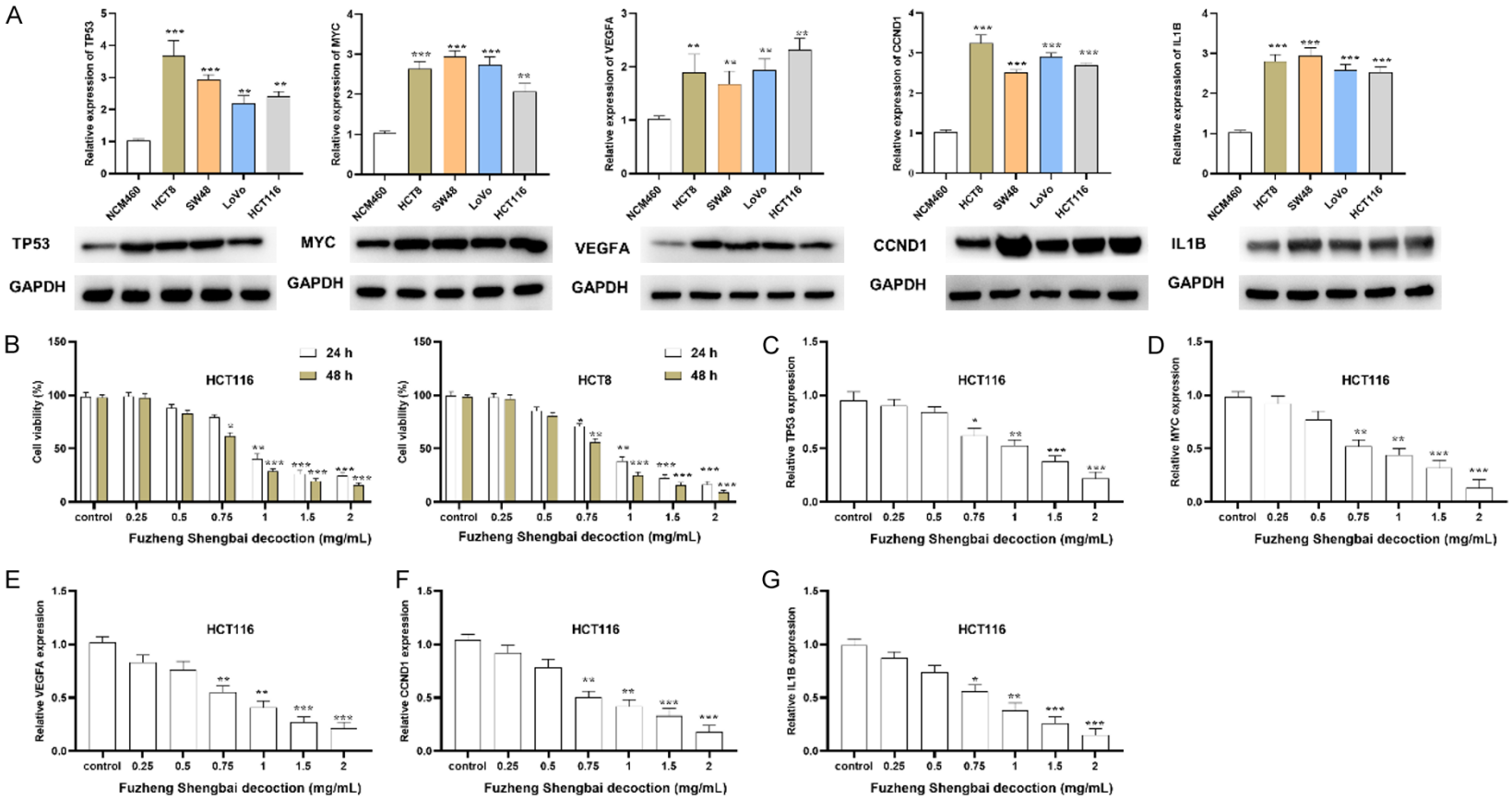

Figure 5. FZSBD inhibited the expression of five hub genes and the cell viability of CC cells. A. Real-time quantitative PCR (RT-qPCR) and Western blotting analyses were used to detect the mRNA and protein expression of five hub genes (TP53, MYC, VEGFA, CCND1, and IL1B) in CC cell lines and control cells. B. MTT assays were performed to evaluate the effects of FZSBD on CC cell proliferation at different doses and time points. C-G. RT-qPCR was conducted to evaluate the expression of TP53, MYC, VEGFA, CCND1, and IL1B in CC cells treated with different concentrations of FZSBD. The ANOVA test and Tukey's test were applied for comparison among groups. ***/**/*P<0.001/0.01/0.05 vs. the first group.

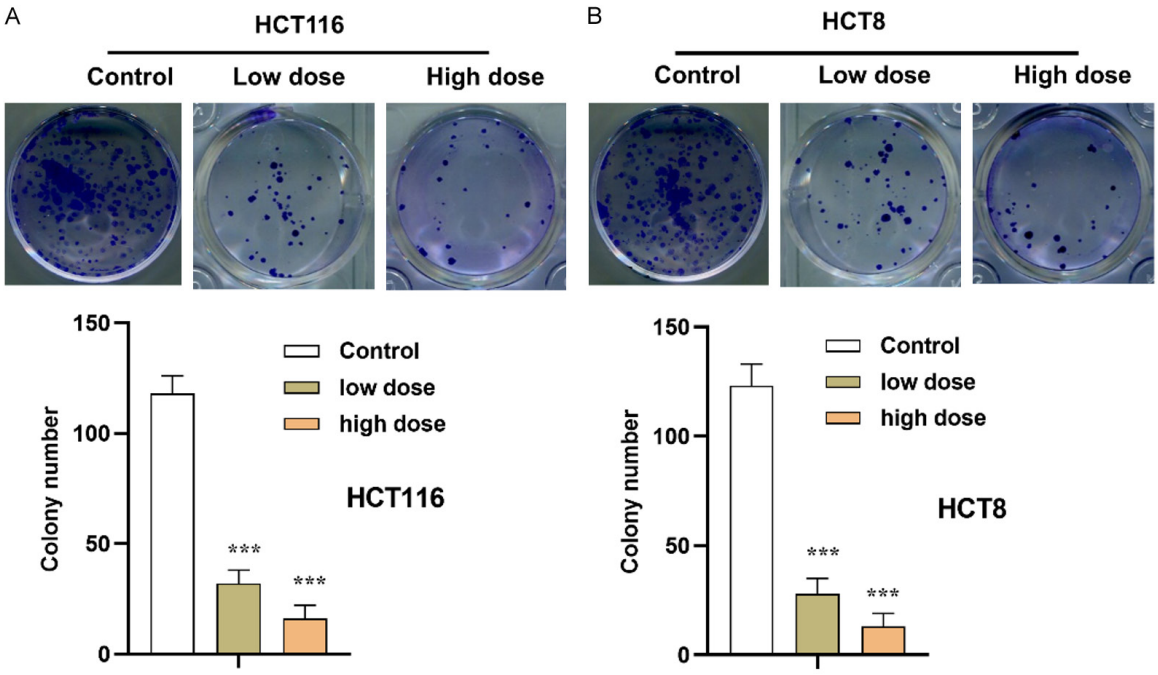

Figure 6. FZSBD suppressed the proliferation of CC cells. A, B. Colony formation assays were used to evaluate the proliferation ability of CC cells with low dose (0.75 mg/mL) or high dose (1.5 mg/mL) of treatment with FZSBD. The ANOVA test and Tukey's test were applied for the comparison among groups. ***P<0.001 vs. the first group.

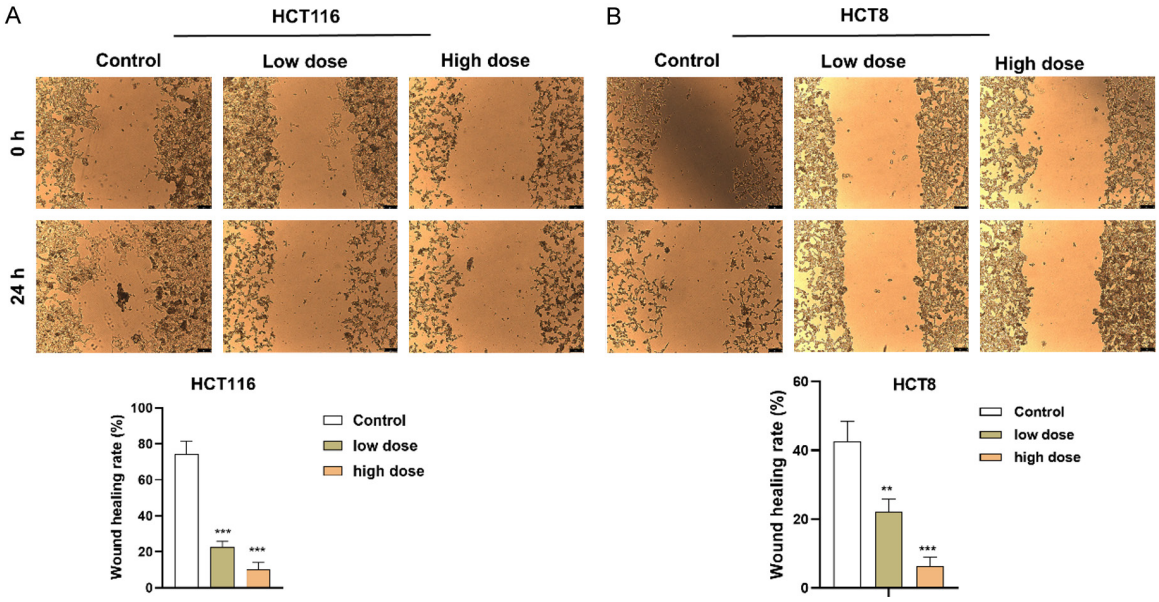

Figure 7. The effects of FZSBD on cell migration of CC. A, B. Wound healing assays were performed to evaluate the impact of FZSBD at low or high doses on the migration ability of CC cells. The ANOVA test and Tukey's test were applied for the comparison among groups. ***/**P<0.001/0.01 vs. the first group.

FZSB manifested a more profound decrease in CRP and TNF-α compared to using XELOX alone, suggesting superiority of the combined treatment for attenuating systemic inflammation. In conclusion, although both therapies affected hematological, immunological, and inflammatory data, the addition of FZSB to the XELOX regimen appeared to enhance immune modu-

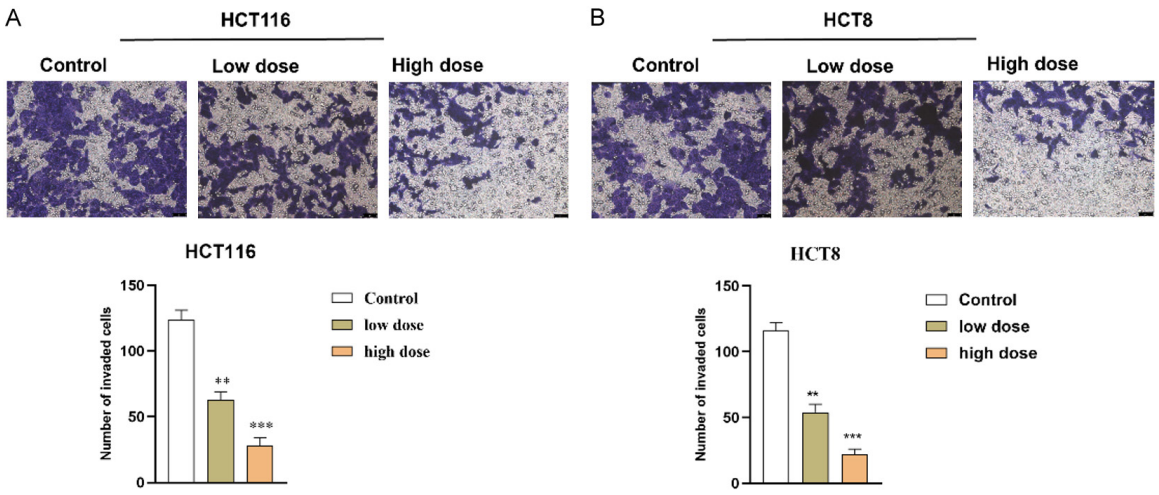

Figure 8. The effects of FZSBD on cell invasion of CC. A. B. Transwell assays were conducted to examine the invasion ability of HCT116 and HCT8 cells in each group. The ANOVA test and Tukey's test were applied for the comparison among groups. ***/**P<0.001/0.01 vs. the first group.

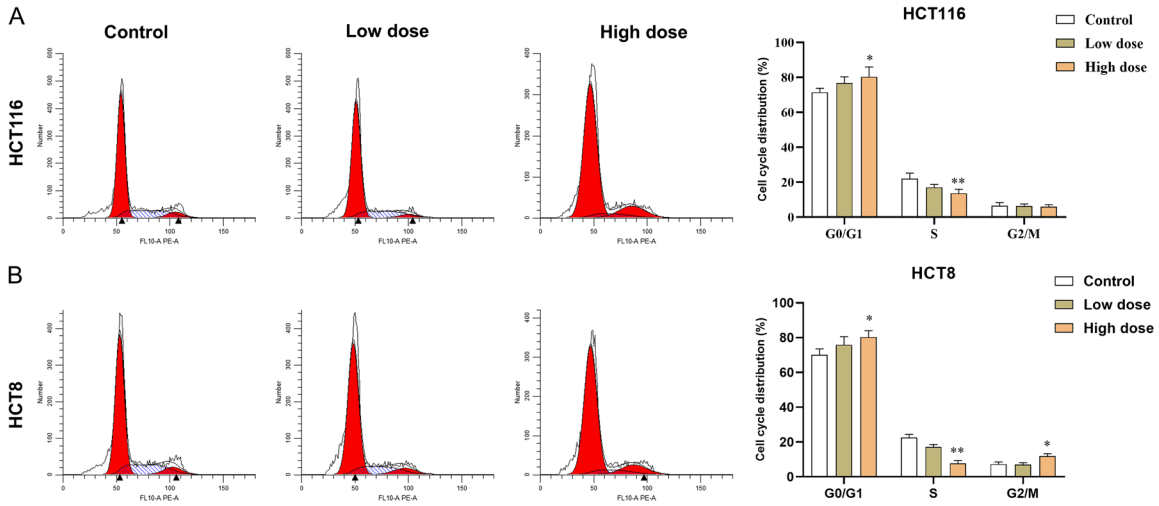

Figure 9. The effects of FZSBD on cell cycle processes of CC cells. A, B. Flow cytometry was used to examine the cell cycle processes of HCT116 and HCT8 cells treated with low or high doses of FZSBD. The ANOVA test and Tukey's test were applied for the comparison among groups. **/*P<0.01/0.05 vs. the first group.

lation and alleviate inflammatory responses, potentially providing benefits in the clinical treatment of CC.

Discussion

In the current study, the active ingredients and corresponding target genes of FZSBD in the treatment of CC were identified. TP53, MYC, VEGFA, CCND1, and IL1B were the five hub genes selected from the PPI network, and they also showed enrichment in the cell cycle process. The subsequent analysis revealed that TP53, MYC, VEGFA, CCND1, and IL1B were of diagnostic value in CC, and were up-regulated in CC tissues and cells. Additionally, TP53, MYC, VEGFA, CCND1, and IL1B were significantly correlated with immune cell infiltration, which was aligned with the observations of hematological, immunological, and inflammatory Data post-treatment. The results of functional assays revealed that the treatment of FZSBD significantly inhibited cell viability, proliferation, migration, invasiveness, and the cell cycle process of CC cells in a dose-dependent way. In addition, the combined regimen of XELOX and

Table 2. Comparison of therapeutic efficacy of XELOX and XELOX + FZSBD regimens in patients with CC

Variable (%)	XELOX	XELOX + FZSBD	χ^2	*P*
CR	6 (26.1)	5 (21.7)	0.0	1.0
PR	8 (34.8)	9 (39.1)	0.0	1.0
SD	4 (17.4)	7 (30.4)	0.478	0.489
DCR	18 (78.3)	21 (91.3)	0.674	0.412
ORR	14 (60.9)	14 (60.9)	0.0	1.0
BMS	16 (69.6)	8 (34.8)*	4.269	0.039
Reduction of CEA (ng/mL)	3.3 ± 5.9	3.9 ± 4.5		0.429

Notes: n = 23 each group. CR, complete response; PR, partial response; SD, stable disease; DCR, disease control rate; ORR, objective response rate; BMS, bone marrow suppression; CEA, carcinoembryonic antigen. For the continuous variables, data are shown as mean ± SD, and the Student's *t*-test and Tukey's test were applied for the comparison between groups. For categorical variables, data are shown as n (%) and the Chi-square test was used for comparison. **P*<0.05.

Table 3. Comparison of peripheral blood values before and after treatment in patients with CC

	XELOX		XELOX + FZSBD	
	Pre-treatment	Post-treatment	Pre-treatment	Post-treatment
WBCs (10^9/L)	4.26 ± 0.46	3.18 ± 0.24***	4.30 ± 0.22	3.13 ± 0.76***
HB (g/L)	123.68 ± 44.32	98.41 ± 41.19	122.39 ± 57.71	103.45 ± 56.12
RBCs (10^{12}/L)	4.91 ± 0.87	3.81 ± 0.36***	4.88 ± 0.71	4.01 ± 054**
PLTs (10^9/L)	205.68 ± 68.69	153.16 ± 61.33**	208.01 ± 64.49	161.11 ± 60.35**

Notes: n = 23 each group. Data are shown as mean ± SD. The Student's *t*-test and Tukey's test were applied for comparison between groups. ***/****P*<0.001/0.01 vs. the pre-treatment group. WBCs, white blood cells; RBCs, red blood cells; PLTs, platelets; HB, hemoglobin.

Table 4. Proportions of T-cell subsets before and after treatment in patients with CC

Subsets (%)	XELOX		XELOX + FZSBD	
	Pre-treatment	Post-treatment	Pre-treatment	Post-treatment
$CD4^+$	40.32 ± 4.33	44.98 ± 5.85**	39.82 ± 4.16	49.23 ± 4.25**
$CD8^+$	25.77 ± 2.57	23.06 ± 3.19*	25.54 ± 2.60	20.98 ± 2.91**,#
$CD4^+/CD8^+$	1.43 ± 0.11	1.76 ± 0.43	1.48 ± 0.26	1.91 ± 0.22*
$CD3^+$	67.09 ± 0.87	69.57 ± 0.36*	66.92 ± 0.71	72.52 ± 1.54**,#

Notes: n = 23 each group. Data are shown as mean ± SD. The Student's *t*-test and Tukey's test were applied for the comparison between groups. **/***P*<0.01/0.05 vs. the pre-treatment group; #*P*<0.05 vs. the post-treatment group of XELOX.

Table 5. Concentrations of inflammatory markers before and after treatment in patients with CC

Marker	XELOX		XELOX + FZSBD	
	Pre-treatment	Post-treatment	Pre-treatment	Post-treatment
CRP (mg/L)	18.25 ± 4.79	14.53 ± 5.23**	18.54 ± 5.02	10.23 ± 4.25***,#
IL-6 (pg/mL)	5.62 ± 2.18	4.02 ± 2.47*	5.81 ± 2.35	4.95 ± 2.23
TNF-α (pg/mL)	25.11 ± 6.59	22.75 ± 6.97	24.92 ± 6.70	17.45 ± 6.38***,#
IL-1β (pg/mL)	12.34 ± 3.27	7.40 ± 3.58***	12.57 ± 3.43	6.75 ± 3.15***

Notes: n = 23 each group. Data are shown as mean ± SD. The Student's *t*-test and Tukey's test were applied for the comparison between groups. ***/**/***P*<0.001/0.01/0.05 vs. the pre-treatment group; #*P*<0.05 vs. the post-treatment group of XELOX. CRP, C-reactive protein; IL-6, interleukin-6; TNF-α, tumor necrosis factor-α; IL-1β, interleukin-1β.

FZSBD improved the modulation of immune and inflammatory responses, reflecting the potential synergy between FZSBD and conventional therapies in the treatment of CC.

Some TCM formulas with high safety and extensive experience in pharmacological applications have shown enormous potential in the treatment of CC [32-34]. FZSBD, a formula developed in our hospital, is composed of nine drugs. *Astragalus membranaceus* (Huangqi) improves the immune system and metabolic functions and possesses anti-inflammatory, immune-regulatory, and anti-tumor activities [35-37]. *Psoralen corylifolia L.* (Buguzhi) has commonly been used to treat bone-related diseases, such as osteoporosis, and also possesses anti-cancer activity [38, 39]. *Cervi Cornus Colla* (Lujiaojiao) has been indicated to have a warm nature, warm the liver and kidney, and replenish vital essence and blood to reinforce the body [40]. Moreover, Lujiaojiao exhibits its effects on the blood circulation and has anti-inflammatory, analgesic, anti-hyperplasia, and gastric mucosal protection activities [41]. Modern pharmacological studies have suggested that Dangshen has antioxidant, antimicrobial, anti-cancer, and cellular immunity improvement properties [42, 43]. Extracts from *Codonopsis pilosula* (Dangshen) inhibit cancer proliferation and migration [11, 44]. *Fructus Ligustri Lucidi* (Nvzhenzi) inhibits inflammation and promotes restoration of the microbiome in colitis, and its extracts also have anti-tumor effects against glioma and CC cells [45, 46]. *Asini Corii Colla* (Ejiao) possesses anti-inflammatory and immune-enhancing effects [47, 48]. Furthermore, Fufang E'jiao Jiang, a prescription of TCM, has been reported to alleviate mucosal injury in gastric cancer by suppressing the inflammatory response and also possesses a hematopoietic effect in chemotherapy-induced myelosuppression mouse models [49]. Danggui Buxue Decoction, a TCM prescription, has shown potential in the treatment of CC, among which *Angelicae Sinensis Radix* (Danggui) was suggested to achieve marked anti-tumor activities [17, 50]. The extract of *Caulis Spatholobi Caulis* (Jixueteng) inhibits CC metastasis by regulating tumor cell-induced platelet aggregation [20]. *Fructus amomi* (Sharen) alleviates 5-fluorouracil-induced intestinal mucositis by suppressing inflammation and strengthening the intestinal mucosal barrier [51]. *Fructus amomi* has also been shown to inhibit cell growth and accelerate apoptosis in gastric cancer [52]. In the present study, we developed a self-made prescription by using these nine drugs, FZSBD. Based on network pharmacology, we identified 109 active components and 912 predicted targets of the nine drugs. The DEGs in CC included 1,364 up-regulated genes and 1,401 down-regulated genes. After DEGs were intersected with drug targets, a total of 184 drug-disease targets were identified. GSEA analysis revealed that these drug-disease targets were enriched in platelet activation signaling and aggregation, extracellular matrix organization, response to platelet cytosolic CA2 elevation, intestinal immune network for IGA production, interferon gamma response, HEME metabolism, epithelial-mesenchymal transition, and the apical junction, which are suggested to be correlated with the immune network.

Furthermore, five hub genes (TP53, MYC, VEGFA, CCND1, and IL1B) were selected from the PPI network. TP53 is a cancer suppressor gene, whose loss or mutation is a prevalent genetic lesion of human cancer [53]. The mutation of TP53 is crucially involved in the development of CC [54]. Wild-type TP53 regulates cell-cycle arrest and cell-death checkpoint by activating cellular stress signals [55]. MYC, a critical oncogene located on chromosome 8q24, is involved in the regulation of cell multiplication, differentiation, and apoptosis [56]. MYC exerts oncogenic effects by regulating the kynurenine pathway to facilitate the uptake and metabolism of tryptophan, especially in CC [57]. A previous study has also revealed that LINC00941 accelerates CC cell proliferation and invasion by activating MYC [58]. VEGFA is crucially involved in cancer angiogenesis and metastasis [59]. MiR-503-5p has been reported to suppress CC tumor growth, angiogenesis, and lymphangiogenesis by negatively regulating VEGFA [60]. Furthermore, miR-299-3p can suppress CC proliferation and invasion by targeting VEGFA [61]. CCND1 encodes cyclin D1 to modulate the cell cycle, which plays an oncogenic role in cancer progression. TRAF6 was reported to facilitate CC cell proliferation by regulating cyclin D1 [62, 63]. IL1B, an inflammation mediator, is frequently up-regulated in various tumors and predicts an adverse prognosis [64]. Furthermore, IL1B improves cell stemness and invasion of CC by activating Zeb1 [65]. In this study, these five hub genes were revealed to be highly expressed in CC based on bioinformatic analysis. KEGG and GO analyses indicated that these genes were enriched in the cell cycle pro-

cess, regulation of kinase, and cancer progression. Moreover, based on the results of bioinformatic analysis, the five hub genes also showed a significant correlation with immune modulation.

Subsequently, the results of cellular experiments *in vitro* further demonstrated that these five hub genes were prominently up-regulated in CC cell lines and the treatment with FZSBD gradually decreased their expression level in a dose-dependent fashion. In addition, FZSBD treatment also significantly decreased cell viability, proliferation, migration, invasion, and induced cell cycle arrest in the G1 phase of CC cells. Furthermore, this study also compared the therapeutic efficacy of the XELOX treatment group and the XELOX + FZSBD treatment group. Although the addition of FZSBD increased the CR, the change was not statistically significant, which may be attributed to the limited sample size. More importantly, the value of BMS in the XELOX treatment group was prominently lower than that in the XELOX + FZSBD group, indicating that the addition of FZSBD significantly reduced the side effects of XELOX. Subsequently, our clinical trial further emphasized the possible effect of FZSBD on inflammatory infiltration and immune modulation. Although hematological parameters declined in both the XELOX treatment and XELOX + FZSBD treatment groups, the $CD3^+$ population increased significantly and the $CD8^+$ population decreased significantly with the addition of FZSB to the regimen. Compared to the single treatment of XELOX, the combined therapy of XELOX with FZSBD also manifested a more profound reduction in inflammatory markers, including CRP and TNF-α, which highlights the potential of FZSBD for attenuating systemic inflammation. Thus, FZSBD not only directly affects the tumor environment but also contributes to improving the systemic inflammatory response in patients.

This study completes the identification of molecular targets and underlying mechanisms of FZSBD against CC based on network pharmacology. The flow diagram is presented in **Figure 10**. Although network pharmacology effectively compensates for the shortcomings of a single target and low selectivity of Chinese materia medica, it still faces some challenges in its practical application [66]. A perfectly constructed database is essential to ensure the accuracy of results of the network pharmacology as the analysis is based on databases and analysis software. Although multiple databases, such as TCMSP, HERB, BATMAN, and UniPort were interrogated in this study, due to limited technological capabilities at present, some databases were incomplete enough. Therefore, the predicted results based on network pharmacology need to be further verified through experiments. Although the gene expression level of the five hub genes in CC cells after being treated with FZSBD was determined in this manuscript, the protein expression level of the five hub genes needs to be further verified, which is a limitation of this study. Moreover, the active ingredients of some Chinese materia medica screened by using network pharmacology in this study might not be the main quality control components, nor the components with highest content, which deserves further examination. The investigation of network pharmacology does not consider one significant element, the dosage or concentration of medications, since the effects of medications on diseases appear only if they reach a certain dosage or concentration [67]. Therefore, it is necessary to determine whether FZSBD at a certain dosage or concentration exerts its therapeutic effects on CC by regulating the five hub genes through experiments *in vivo* and *in vitro*. Although there are some flaws in network pharmacology, the qRT-PCR results indicated that the gene expression levels of TP53, MYC, VEGFA, CCND1, and IL1B were significantly down-regulated in HCT116 cells, which directly reflects the reliability of the predicted results based on network pharmacology in the present manuscript. Network pharmacology results may be more convincing when combined with molecular docking technology or experimental research *in vivo* and *in vitro*. Thus, more detailed pharmacologic studies to verify potential molecular targets and underlying mechanisms of FZSBD in the treatment of CC will be main directions for future studies once network pharmacology has been established.

Conclusions

TP53, MYC, VEGFA, CCND1, and IL1B were five hub genes associated with FZSBD activity in treating CC. The hub genes were enriched in the cell cycle process and cancer progression and were associated with immune modulation

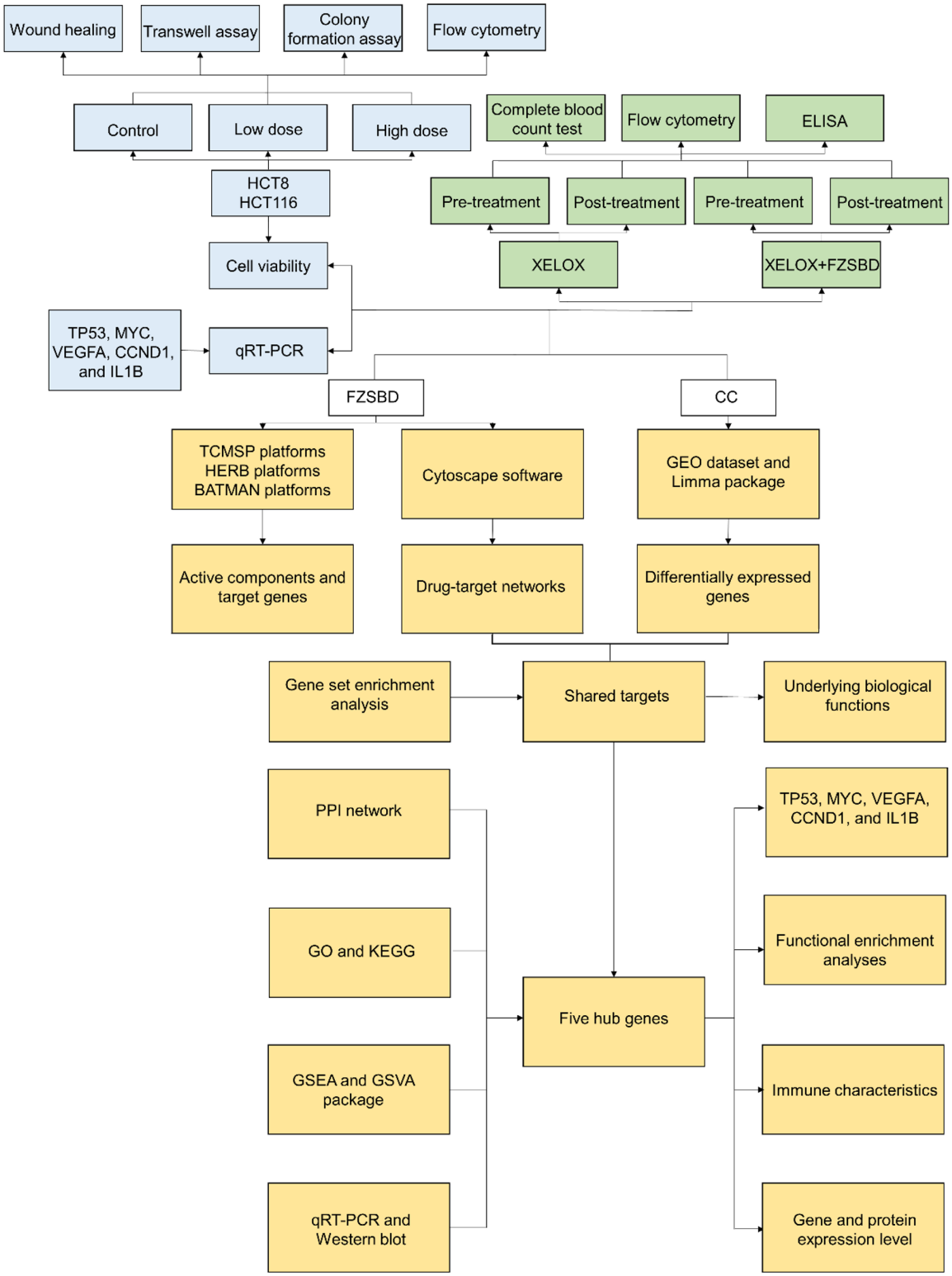

Figure 10. The flow diagram of the present study. Based on network pharmacology, the drug-target network of FZSBD, DEGs of CC, shared targets between FZSBD and CC and their underlying mechanisms, five hub genes (including TP53, MYC, VEGFA, CCND1, and IL1B) and their underlying mechanisms were identified. Next, the effects of FZSBD on the expression levels of the five hub genes in CC cells, cell viability, invasion, migration, proliferation, and on cell cycle of HCT8 and HCT116 cells were further investigated. The effects of FZSBD based on XELOX on the immune microenvironment and inflammatory levels of patients with CC were subsequently investigated.

and inflammatory infiltration based on network pharmacology. In this study, FZSBD possessed anti-tumor effects by regulating cell viability, proliferation, migration, invasion, cell cycle processes, and the expression levels of these five hub genes in CC cells in a dose-dependent manner. FZSBD was also confirmed to improve the therapeutic efficacy of XELOX and regulate T-cell subpopulations and inflammatory markers through clinical trials. The results of our work may deepen the understanding of FZSBD in treating CC.

Acknowledgements

This study was supported by Nanjing Youth Talent Training Project of Traditional Chinese Medicine (No. NJSZYYQNRC-2020-WY-ZYQ20-045).

The written informed consent was obtained from the participation of patients in this study.

Disclosure of conflict of interest

None.

Address correspondence to: Mingzhi Fang, Department of Oncology, Nanjing Hospital of Traditional Chinese Medicine, No. 157, Daming Road, Qinhuai District, Nanjing 210022, Jiangsu, China. E-mail: fangmingzhi025@vip.163.com; Qin Zheng, Department of Oncology, Nanjing Hospital Affiliated to Nanjing University of Chinese Medicine, No. 1-1, Zhongfu Road, Nanjing 210003, Jiangsu, China. E-mail: njzq83626472@sina.com

References

[1] Sung H, Ferlay J, Siegel RL, Laversanne M, Soerjomataram I, Jemal A and Bray F. Global cancer statistics 2020: GLOBOCAN estimates of incidence and mortality worldwide for 36 cancers in 185 countries. CA Cancer J Clin 2021; 71: 209-249.

[2] Chuang JP, Tsai HL, Chen PJ, Chang TK, Su WC, Yeh YS, Huang CW and Wang JY. Comprehensive review of biomarkers for the treatment of locally advanced colon cancer. Cells 2022; 11: 3744.

[3] Favoriti P, Carbone G, Greco M, Pirozzi F, Pirozzi RE and Corcione F. Worldwide burden of colorectal cancer: a review. Updates Surg 2016; 68: 7-11.

[4] Li Z, Feiyue Z and Gaofeng L. Traditional Chinese medicine and lung cancer–from theory to practice. Biomed Pharmacother 2021; 137: 111381.

[5] Xu W, Li B, Xu M, Yang T and Hao X. Traditional Chinese medicine for precancerous lesions of gastric cancer: a review. Biomed Pharmacother 2022; 146: 112542.

[6] Nie X, Geng Z, Liu J, Qi L, Wang Z, Liu T and Tang J. Chinese herbal medicine anticancer cocktail soup activates immune cells to kill colon cancer cells by regulating the gut microbiota-Th17 axis. Front Pharmacol 2022; 13: 963638.

[7] Wu X, Yang H, Chen X, Gao J, Duan Y, Wei D, Zhang J, Ge K, Liang XJ, Huang Y, Feng S, Zhang R, Chen X and Chang J. Nano-herb medicine and PDT induced synergistic immunotherapy for colon cancer treatment. Biomaterials 2021; 269: 120654.

[8] Ziyang T, Xirong H, Chongming A and Tingxin L. The potential molecular pathways of Astragaloside-IV in colorectal cancer: a systematic review. Biomed Pharmacother 2023; 167: 115625.

[9] Li Q, Zhang C, Xu G, Shang X, Nan X, Li Y, Liu J, Hong Y, Wang Q and Peng G. Astragalus polysaccharide ameliorates CD8(+) T cell dysfunction through STAT3/Gal-3/LAG3 pathway in inflammation-induced colorectal cancer. Biomed Pharmacother 2024; 171: 116172.

[10] Chopra B, Dhingra AK and Dhar KL. Psoralea corylifolia L. (Buguchi) - folklore to modern evidence: review. Fitoterapia 2013; 90: 44-56.

[11] Xin T, Zhang F, Jiang Q, Chen C, Huang D, Li Y, Shen W, Jin Y and Sui G. The inhibitory effect of a polysaccharide from Codonopsis pilosula on tumor growth and metastasis in vitro. Int J Biol Macromol 2012; 51: 788-93.

[12] Bai R, Li W, Li Y, Ma M, Wang Y, Zhang J and Hu F. Cytotoxicity of two water-soluble polysaccharides from Codonopsis pilosula Nannf. var. modesta (Nannf.) L.T.Shen against human hepatocellular carcinoma HepG2 cells and its mechanism. Int J Biol Macromol 2018; 120: 1544-1550.

[13] Salamatullah AM, Subash-Babu P, Nassrallah A, Alshatwi AA and Alkaltham MS. Cyclotrisiloxan and β-Sitosterol rich Cassia alata (L.) flower inhibit HT-115 human colon cancer cell growth via mitochondrial dependent apoptotic stimulation. Saudi J Biol Sci 2021; 28: 6009-6016.

[14] Makran M, Garcia-Llatas G, Alegría A and Cilla A. Ethylcoprostanol modulates colorectal cancer cell proliferation and mitigates cytotoxicity of cholesterol metabolites in non-tumor colon cells. Food Funct 2023; 14: 10829-10840.

[15] Xu X, Guo S, Hao X, Ma H, Bai Y and Huang Y. Improving antioxidant and antiproliferative activities of colla corii asini hydrolysates using

ginkgo biloba extracts. Food Sci Nutr 2018; 6: 765-772.
[16] Wu H, Ren C, Yang F, Qin Y, Zhang Y and Liu J. Extraction and identification of collagen-derived peptides with hematopoietic activity from Colla Corii Asini. J Ethnopharmacol 2016; 182: 129-36.
[17] Feng SH, Zhao B, Zhan X, Motanyane R, Wang SM and Li A. Danggui buxue decoction in the treatment of metastatic colon cancer: network pharmacology analysis and experimental validation. Drug Des Devel Ther 2021; 15: 705-720.
[18] Chen XP, Li W, Xiao XF, Zhang LL and Liu CX. Phytochemical and pharmacological studies on Radix Angelica sinensis. Chin J Nat Med 2013; 11: 577-87.
[19] Chen X, Li Q, Kan XX, Wang YJ, Li YJ, Yang Q, Xiao HB, Chen Y, Weng XG, Cai WY and Zhu XX. Extract of Caulis Spatholobi, a novel blocker targeting tumor cell-induced platelet aggregation, inhibits breast cancer metastasis. Oncol Rep 2016; 36: 3215-3224.
[20] Sun L, Li Q, Guo Y, Yang Q, Yin J, Ran Q, Liu L, Zhao Z, Wang Y, Li Y, Chen Y, Weng X, Cai W and Zhu X. Extract of Caulis Spatholobi, a novel platelet inhibitor,efficiently suppresses metastasis of colorectal cancer by targeting tumor cell-induced platelet aggregation. Biomed Pharmacother 2020; 123: 109718.
[21] Nogales C, Mamdouh ZM, List M, Kiel C, Casas AI and Schmidt HHHW. Network pharmacology: curing causal mechanisms instead of treating symptoms. Trends Pharmacol Sci 2022; 43: 136-150.
[22] Li S and Zhang B. Traditional Chinese medicine network pharmacology: theory, methodology and application. Chin J Nat Med 2013; 11: 110-20.
[23] Yang J, Tian S, Zhao J and Zhang W. Exploring the mechanism of TCM formulae in the treatment of different types of coronary heart disease by network pharmacology and machining learning. Pharmacol Res 2020; 159: 105034.
[24] Chen Z, Wang X, Li Y, Wang Y, Tang K, Wu D, Zhao W, Ma Y, Liu P and Cao Z. Comparative network pharmacology analysis of classical TCM prescriptions for chronic liver disease. Front Pharmacol 2019; 10: 1353.
[25] Yu S, Gao W, Zeng P, Chen C, Zhang Z, Liu Z and Liu J. Exploring the effect of Gupi Xiaoji Prescription on hepatitis B virus-related liver cancer through network pharmacology and in vitro experiments. Biomed Pharmacother 2021; 139: 111612.
[26] Gao P and Ren G. Identification of potential target genes of non-small cell lung cancer in response to resveratrol treatment by bioinformatics analysis. Aging (Albany NY) 2021; 13: 23245-23261.
[27] Liu H, Hu Y, Qi B, Yan C, Wang L, Zhang Y and Chen L. Network pharmacology and molecular docking to elucidate the mechanism of pulsatilla decoction in the treatment of colon cancer. Front Pharmacol 2022; 13: 940508.
[28] Ru J, Li P, Wang J, Zhou W, Li B, Huang C, Li P, Guo Z, Tao W, Yang Y, Xu X, Li Y, Wang Y and Yang L. TCMSP: a database of systems pharmacology for drug discovery from herbal medicines. J Cheminform 2014; 6: 13.
[29] Fang S, Dong L, Liu L, Guo J, Zhao L, Zhang J, Bu D, Liu X, Huo P, Cao W, Dong Q, Wu J, Zeng X, Wu Y and Zhao Y. HERB: a high-throughput experiment- and reference-guided database of traditional Chinese medicine. Nucleic Acids Res 2021; 49: D1197-D1206.
[30] Liu Z, Guo F, Wang Y, Li C, Zhang X, Li H, Diao L, Gu J, Wang W, Li D and He F. BATMAN-TCM: a bioinformatics analysis tool for molecular mechANism of traditional Chinese medicine. Sci Rep 2016; 6: 21146.
[31] Peng W, Zhang S, Zhang Z, Xu P, Mao D, Huang S, Chen B, Zhang C and Zhang S. Jianpi Jiedu decoction, a traditional Chinese medicine formula, inhibits tumorigenesis, metastasis, and angiogenesis through the mTOR/HIF-1α/VEGF pathway. J Ethnopharmacol 2018; 224: 140-148.
[32] Kim J, Kim HY, Hong S, Shin S, Kim YA, Kim NS and Bang OS. A new herbal formula BP10A exerted an antitumor effect and enhanced anticancer effect of irinotecan and oxaliplatin in the colon cancer PDTX model. Biomed Pharmacother 2019; 116: 108987.
[33] Sui H, Zhang L, Gu K, Chai N, Ji Q, Zhou L, Wang Y, Ren J, Yang L, Zhang B, Hu J and Li Q. YYFZBJS ameliorates colorectal cancer progression in Apc(Min/+) mice by remodeling gut microbiota and inhibiting regulatory T-cell generation. Cell Commun Signal 2020; 18: 113.
[34] Liu H, Liu H, Zhou Z, Parise RA, Chu E and Schmitz JC. Herbal formula Huang Qin Ge Gen Tang enhances 5-fluorouracil antitumor activity through modulation of the E2F1/TS pathway. Cell Commun Signal 2018; 16: 7.
[35] Ryu M, Kim EH, Chun M, Kang S, Shim B, Yu YB, Jeong G and Lee JS. Astragali Radix elicits anti-inflammation via activation of MKP-1, concomitant with attenuation of p38 and Erk. J Ethnopharmacol 2008; 115: 184-93.
[36] Nalbantsoy A, Nesil T, Yılmaz-Dilsiz O, Aksu G, Khan S and Bedir E. Evaluation of the immunomodulatory properties in mice and in vitro anti-inflammatory activity of cycloartane type saponins from Astragalus species. J Ethnopharmacol 2012; 139: 574-81.

[37] Qin J, Wang W, Sha L and Ge L. Huangqi Fuzheng decoction exerts antitumor activity by inhibiting cell growth and inducing cell death in osteosarcoma. Biomed Pharmacother 2019; 114: 108854.
[38] Wong RW and Rabie AB. Effect of Buguzhi (Psoralea corylifolia fruit) extract on bone formation. Phytother Res 2010; 24 Suppl 2: S155-60.
[39] Ren Y, Song X, Tan L, Guo C, Wang M, Liu H, Cao Z, Li Y and Peng C. A review of the pharmacological properties of psoralen. Front Pharmacol 2020; 11: 571535.
[40] Wu MH, Huang Y, Xu HK, Xie Y, Zhang T, Ma ZG, Zhang Y and Cao H. Herbalogical study on Cervi Colla. Zhongguo Zhong Yao Za Zhi 2020; 45: 1188-1193.
[41] Bao Y, Gao JT, Sun JM and Zhang H. Research progress of traditional Chinese medicine Colla Corni Cervi. Jilin J Tradit Chin Med 2016; 36: 173-175, 204.
[42] Han AY, Lee YS, Kwon S, Lee HS, Lee KW and Seol GH. Codonopsis lanceolata extract prevents hypertension in rats. Phytomedicine 2018; 39: 119-124.
[43] Qin T, Ren Z, Liu X, Luo Y, Long Y, Peng S, Chen S, Zhang J, Ma Y, Li J and Huang Y. Study of the selenizing Codonopsis pilosula polysaccharides protects RAW264.7 cells from hydrogen peroxide-induced injury. Int J Biol Macromol 2019; 125: 534-543.
[44] Chen M, Li Y, Liu Z, Qu Y, Zhang H, Li D, Zhou J, Xie S and Liu M. Exopolysaccharides from a Codonopsis pilosula endophyte activate macrophages and inhibit cancer cell proliferation and migration. Thorac Cancer 2018; 9: 630-639.
[45] Jeong JC, Kim JW, Kwon CH, Kim TH and Kim YK. Fructus ligustri lucidi extracts induce human glioma cell death through regulation of Akt/mTOR pathway in vitro and reduce glioma tumor growth in U87MG xenograft mouse model. Phytother Res 2011; 25: 429-34.
[46] Zhang JF, He ML, Qi D, Xie WD, Chen YC, Lin MC, Leung PC, Zhang YO and Kung HF. Aqueous extracts of Fructus Ligustri Lucidi enhance the sensitivity of human colorectal carcinoma DLD-1 cells to doxorubicin-induced apoptosis via Tbx3 suppression. Integr Cancer Ther 2011; 10: 85-91.
[47] Zhang G, Guo F, Zeng M, Wang Z, Qin F, Chen J, Zheng Z and He Z. The immune-enhancing effect and in vitro antioxidant ability of different fractions separated from Colla corii asini. J Food Biochem 2022; 46: e14174.
[48] Yue Q, Zhang W, Lin S, Zheng T, Hou Y, Zhang Y, Li Z, Wang K, Yue L, Abay B, Li M and Fan L. Ejiao ameliorates lipopolysaccharide-induced pulmonary inflammation via inhibition of NFκB regulating NLRP3 inflammasome and mitochondrial ROS. Biomed Pharmacother 2022; 152: 113275.
[49] Shi WB, Wang ZX, Liu HB, Jia YJ, Wang YP, Xu X, Zhang Y, Qi XD and Hu FD. Study on the mechanism of Fufang E'jiao Jiang on precancerous lesions of gastric cancer based on network pharmacology and metabolomics. J Ethnopharmacol 2023; 304: 116030.
[50] Chen ST, Lee TY, Tsai TH, Lin YC, Lin CP, Shieh HR, Hsu ML, Chi CW, Lee MC, Chang HH and Chen YJ. The traditional Chinese medicine DangguiBuxue Tang sensitizes colorectal cancer cells to chemoradiotherapy. Molecules 2016; 21: 1677.
[51] Zhang T, Lu SH, Bi Q, Liang L, Wang YF, Yang XX, Gu W and Yu J. Volatile oil from amomi fructus attenuates 5-fluorouracil-induced intestinal mucositis. Front Pharmacol 2017; 8: 786.
[52] Yue J, Zhang S, Zheng B, Raza F, Luo Z, Li X, Zhang Y, Nie Q and Qiu M. Efficacy and mechanism of active fractions in fruit of amomum villosum Lour. for gastric cancer. J Cancer 2021; 12: 5991-5998.
[53] Blagih J, Buck MD and Vousden KH. p53, cancer and the immune response. J Cell Sci 2020; 133: jcs237453.
[54] Nakayama M and Oshima M. Mutant p53 in colon cancer. J Mol Cell Biol 2019; 11: 267-276.
[55] Vazquez A, Bond EE, Levine AJ and Bond GL. The genetics of the p53 pathway, apoptosis and cancer therapy. Nat Rev Drug Discov 2008; 7: 979-87.
[56] Dalla-Favera R, Bregni M, Erikson J, Patterson D, Gallo RC and Croce CM. Human c-myc onc gene is located on the region of chromosome 8 that is translocated in Burkitt lymphoma cells. Proc Natl Acad Sci U S A 1982; 79: 7824-7.
[57] Venkateswaran N, Lafita-Navarro MC, Hao YH, Kilgore JA, Perez-Castro L, Braverman J, Borenstein-Auerbach N, Kim M, Lesner NP, Mishra P, Brabletz T, Shay JW, DeBerardinis RJ, Williams NS, Yilmaz OH and Conacci-Sorrell M. MYC promotes tryptophan uptake and metabolism by the kynurenine pathway in colon cancer. Genes Dev 2019; 33: 1236-1251.
[58] Chang L, Zhou D and Luo S. Novel lncRNA LINC00941 promotes proliferation and invasion of colon cancer through activation of MYC. Onco Targets Ther 2021; 14: 1173-1186.
[59] Claesson-Welsh L and Welsh M. VEGFA and tumour angiogenesis. J Intern Med 2013; 273: 114-27.
[60] Wei L, Sun C, Zhang Y, Han N and Sun S. miR-503-5p inhibits colon cancer tumorigenesis, angiogenesis, and lymphangiogenesis by directly downregulating VEGF-A. Gene Ther 2022; 29: 28-40.

[61] Wang JY, Jiang JB, Li Y, Wang YL and Dai Y. MicroRNA-299-3p suppresses proliferation and invasion by targeting VEGFA in human colon carcinoma. Biomed Pharmacother 2017; 93: 1047-1054.
[62] Sun H, Li X, Fan L, Wu G, Li M and Fang J. TRAF6 is upregulated in colon cancer and promotes proliferation of colon cancer cells. Int J Biochem Cell Biol 2014; 53: 195-201.
[63] Montalto FI and De Amicis F. Cyclin D1 in cancer: a molecular connection for cell cycle control, adhesion and invasion in tumor and stroma. Cells 2020; 9: 2648.
[64] Bent R, Moll L, Grabbe S and Bros M. Interleukin-1 Beta-a friend or foe in malignancies? Int J Mol Sci 2018; 19: 2155.
[65] Li Y, Wang L, Pappan L, Galliher-Beckley A and Shi J. IL-1β promotes stemness and invasiveness of colon cancer cells through Zeb1 activation. Mol Cancer 2012; 11: 87.
[66] Lin F, Zhang G, Yang X, Wang M, Wang R, Wan M, Wang J, Wu B, Yan T and Jia Y. A network pharmacology approach and experimental validation to investigate the anticancer mechanism and potential active targets of ethanol extract of Wei-Tong-Xin against colorectal cancer through induction of apoptosis via PI3K/AKT signaling pathway. J Ethnopharmacol 2023; 303: 115933.
[67] Gao WY, Si N, Li ML, Gu XR, Zhang Y, Zhou YY, Wang HJ, Wei XL, Bian BL and Zhao HY. The integrated study on the chemical profiling and in vivo course to explore the bioactive constituents and potential targets of Chinese classical formula Qingxin Lianzi Yin decoction by UHPLC-MS and network pharmacology approaches. J Ethnopharmacol 2021; 272: 113917.